ACS APPLIED MATERIALS & INTERFACES

Research Article

www.acsami.org

ZnO-Based Microfluidic pH Sensor: A Versatile Approach for Quick Recognition of Circulating Tumor Cells in Blood

Ganesh Kumar Mani,*[,†] Madoka Morohoshi,[‡] Yutaka Yasoda,[‡] Sho Yokoyama,[†] Hiroshi Kimura,[§] and Kazuyoshi Tsuchiya[†,∥]

[†]Micro/Nano Technology Center, [‡]Graduate School of Science and Technology, [§]Department of Mechanical Engineering, and [∥]Department of Precision Engineering, Tokai University, 4-1-1 Kitakaname, Hiratsuka, Kanagawa 259-1292, Japan

ABSTRACT: The present study is concerned about the development of highly sensitive and stable microfluidic pH sensor for possible identification of circulating tumor cells (CTCs) in blood. The precise pH measurements between silver−silver chloride (Ag/AgCl) reference electrode and zinc oxide (ZnO) working electrode have been investigated in the microfluidic device. Since there is a direct link between pH and cancer cells, the developed device is one of the valuable tools to examine circulating tumor cells (CTCs) in blood. The ZnO-based working electrode was deposited by radio frequency (rf) sputtering technique. The potential voltage difference between the working and reference electrodes (Ag/AgCl) is evaluated on the microfluidic device. The ideal Nernstian response of −43.71165 mV/pH was achieved along with high stability and quick response time. Finally, to evaluate the real time capability of the developed microfluidic device, *in vitro* testing was done with A549, A7r5, and MDCK cells.

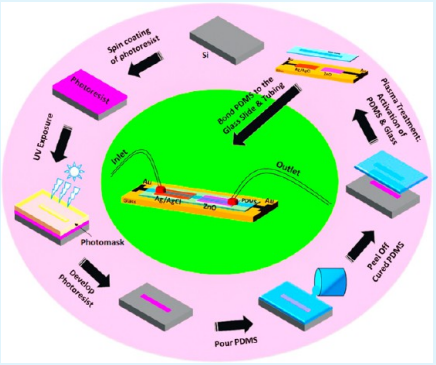

KEYWORDS: *circulating tumor cells, thin films, ZnO, sputtering, pH sensor, in vitro testing*

1. INTRODUCTION

Despite decades of efforts, identification of circulating tumor cells (CTCs) in patient blood remains one of the major challenges in clinical diagnosis. The ability to isolate or identify the rare circulating tumor cells (1−5 CTC in 10^9 cells in 1 mL of blood) has the greater potential in medical field for the early detection of cancer in patients.[1−3] Numerous methods have been developed in recent years to recognize CTCs from the whole blood. However, one of the first and most widely researched CTC identification technique is size-based filtration. The technique is time-consuming and fabrication cost of such recognition devices is quite expensive.[4−6] Moreover, an increasing trend of more cancer deaths daily demands a novel device which can perform better to identify CTCs from blood to identify metastasis. In recent days, a deterministic lateral displacement (DLD)-based microfluidic device has shown versatility to identify CTCs from blood. Antibody-modified microdevices already demonstrated remarkable performances to capture CTCs, but their fabrication complexity limits their usage in clinical laboratories.[7−9] Fortunately, there is plenty of research showing the link between pH and cancer. It is believed that tumor cells can preferentially convert glucose and other substances into lactic acid (pH); hence, it turns the intracellular fluid slightly acidic.[10,11] Generally, the pH of the cancer extracellular environment is known to be 6.2−6.9 compared with 7.3−7.4 of the normal cells. Also, pH values can be used as an indicator for disease diagnostics, medical treatment optimization, and monitoring many biochemical processes inside the body,[12−15] but pH electrode technology has not changed much in the last few decades after the first pH meter constructed by Arnold Beckman in 1934.[16] The conventional glass rod pH sensor has certain disadvantages in clinical applications. Miniaturization of pH sensors for biomedical applications created rapid interest in developing a new type of planar sensors with high sensitivity. Many thick and thin film technologies for pH sensor were developed so far in the last few decades without giving special attention to the miniaturized electrodes. With microfluidic technology, it is possible to deal with very small samples for pH-sensing purposes. A polydimethylsiloxane (PDMS)-based microfluidic device is the material of choice for many researchers due to their low cost and ease of fabrication.[4,7,9,17] Moreover, the advantages of the combined electrodes are easy handling and temperature equality of both electrodes.

Numerous systematic studies of various metal oxides like ZnO,[18−20] WO_3,[21] Ir_2O_3,[22] MnO,[23] and RuO_2[24] as pH sensors have been investigated recent years. Among these, ZnO is a well-known amphoteric oxide which reacts with both acids and bases. In addition, its polar and nonpolar surfaces along with high crystallinity nature makes them one of the potential candidate for pH selective element.[25−29] However, in the previous reports, various types of pH sensors fabricated based on ZnO like potentiometric,[25] surface acoustic wave,[30] resistance[31,32] and extended gate field effect transistor.[33] Kang et al. studied the pH-sensing characteristics of single ZnO nanorod prepared by thermal evaporation technique in the

Received: December 19, 2016
Accepted: January 24, 2017
Published: January 24, 2017

DOI: 10.1021/acsami.6b16261
ACS Appl. Mater. Interfaces 2017, 9, 5193−5203

Table 1. Optimized Deposition Parameters for ZnO and Au Thin Films

parameters	ZnO thin film	Au electrode
substrate	glass	glass
flow rate of Ar gas	50 sccm	80 sccm
sputtering time	60 min	10 min
distance between target and substrate	40 mm	50 mm
microwave power	100 W	100 W

microchannel, but the stable sensing operation of the sensor was achieved only when illuminated with UV rays.[19] Menzel et al. also studied the pH-sensing characteristics of the C4F8 polymer coated ZnO nanowires in a microfluidic platform and achieved the sensitivity of −2.063 μS/pH.[18] Oh et al. also fabricated surface acoustic wave based ZnO nanoparticle pH sensor.[30] A flexible-type pH sensor developed by Maiolo et al. using ZnO nanowalls and achieved the sensitivity near Nernstian response.[34] In most cases, reference electrode was used separately, and there is no detailed characterization about response time and stability. Hence, toward miniaturization we have planned to integrate the reference/working electrodes and microfluidic channels in a single platform. Toward this end, ZnO thin film was grown on glass substrates by radio frequency (rf) sputtering. Previously, ZnO thin films has been grown by many methods such as spray pyrolysis,[35,36] rf/dc sputtering,[37] pulsed laser deposition,[38,39] spin-/dip-coating,[32] hydrothermal,[40] ion beam,[41] and molecular beam epitaxial methods.[42] Sputtering techniques have the distinct advantages of high uniformity, high purity, good adherence, dense coating to the underlying substrate, controlled deposition rate, and high degree of crystallinity.[37,43] Furthermore, Ag/AgCl ink was used as reference electrode on glass substrate instead of a separate Ag/AgCl glass electrode. The advantage of using Ag/AgCl ink as reference electrodes is it can be coated on metal like Au, Ag, Pt, and so on, dries quickly, and is ready to use immediately. Also, the proposed straight single microfluidic channel greatly simplify the design and fabrication of master molds. If complicated patterns are formed on the microfluidic structures, then complicated fabrication processes are required, thereby resulting in high manufacturing costs and time. The fundamental advantage of this channel is reduced consumptions of the reagents, reduced contamination, and highly efficient experimental output. The key technology of this present research work is exploiting the unique pH sensor and biochemical properties of the blood; together with the advancement of the microfluidic devices, we have demonstrated a fabrication of simple and novel microfluidic pH sensor for possible identification of CTCs in blood. Finally, we have evaluated detection range, sensitivity, and durability for long-term experiments.

2. MATERIALS AND METHODS

2.1. Film Deposition. The reference and working electrodes were housed in a thin glass substrate. Prior to electrode deposition, glass substrates were washed with piranha solution to remove organic residues and then with mild detergent (Cica Clean, Kanto Chemical Co. Inc., Japan) in an ultrasonic bath for 30 min. At first, a thin layer of

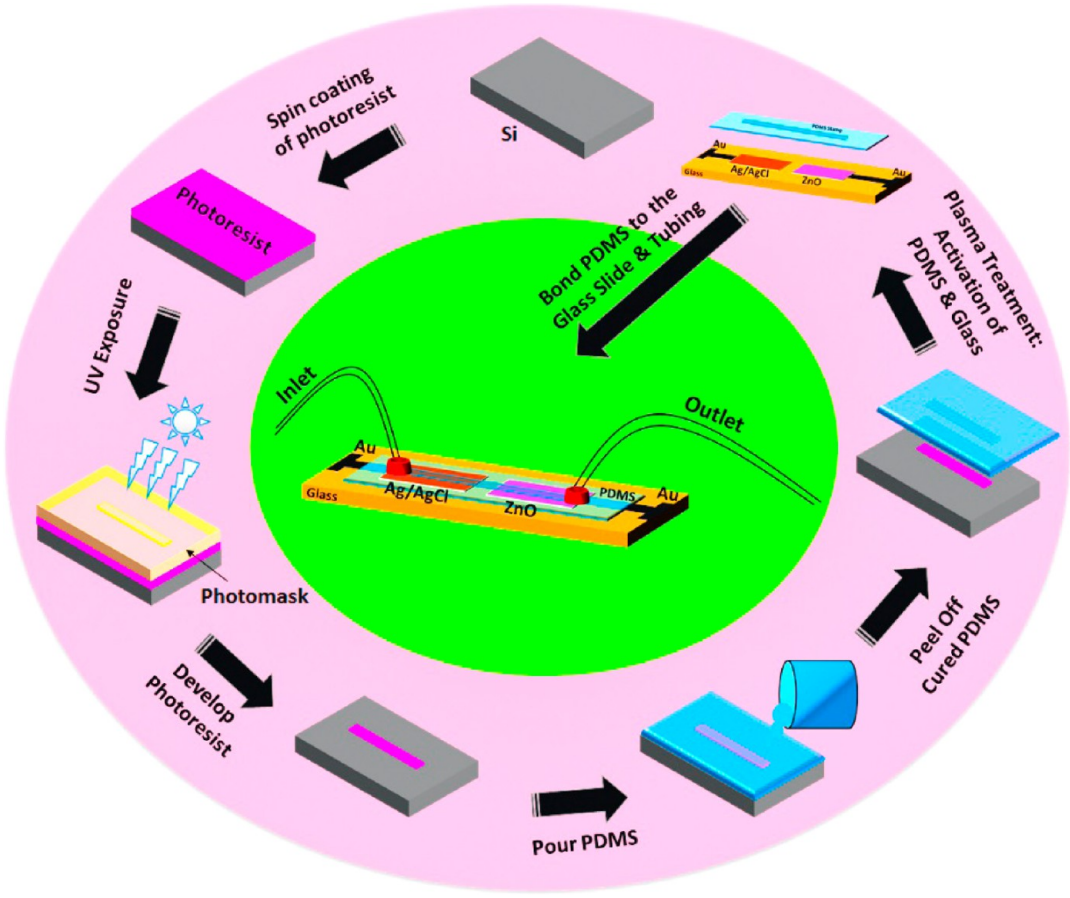

Figure 1. Microfluidic device fabrication scheme.

DOI: 10.1021/acsami.6b16261
ACS Appl. Mater. Interfaces 2017, 9, 5193−5203

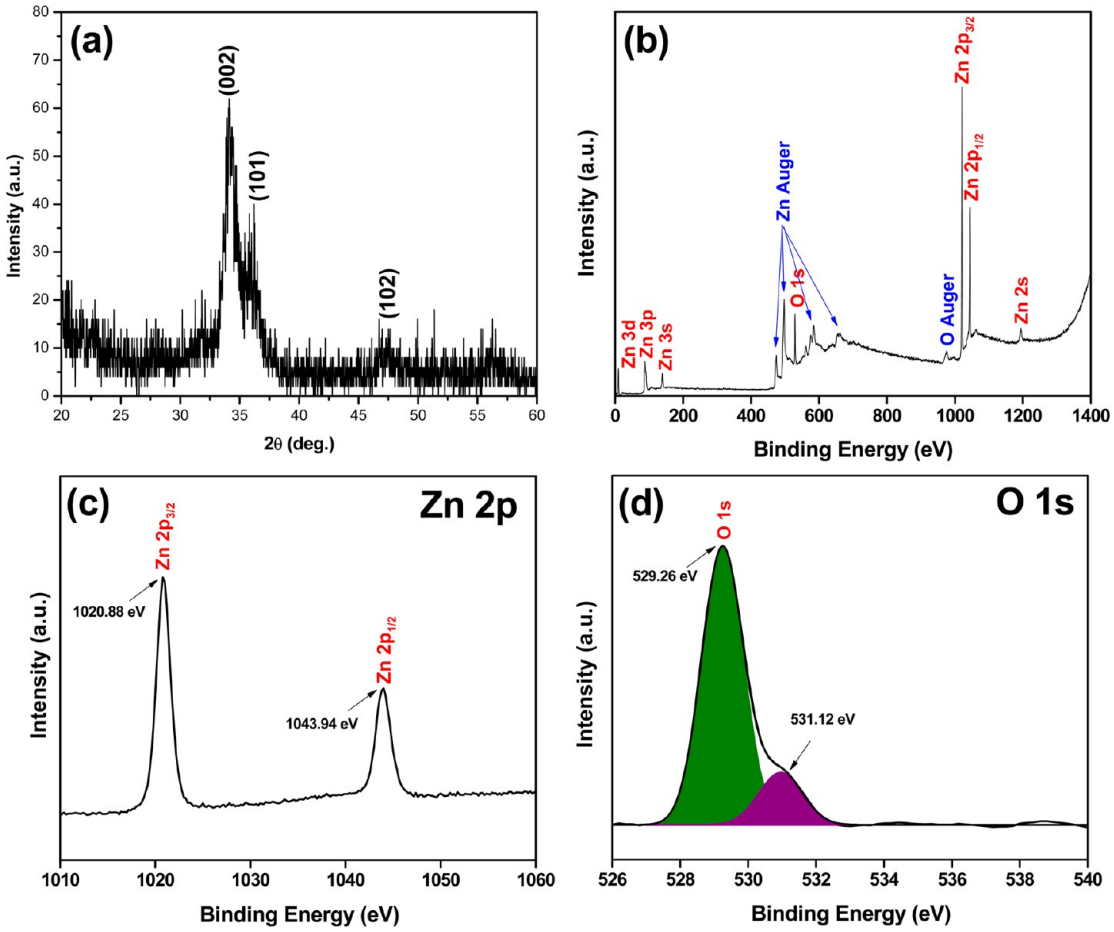

Figure 2. (a) XRD pattern of the ZnO thin film, (b) XPS survey scan spectra, and (c) Zn 2p and (d) O 1s narrow scan spectra of ZnO thin film.

gold (Au) with thickness around ~50 nm was deposited through electron cyclotron resonance (ECR) sputtering as a contact electrodes. The working electrode is made up of 120 nm thick ZnO thin film with the surface area of 5 mm^2 was deposited by rf sputtering technique. Circular ZnO target (Furuuchi Chemical Corporation, Japan; purity of 99.99%.) with 1 in. diameter and 2 mm thickness was used as a source. The reference electrode is made up of 100 μm thick Ag/AgCl ink (ALS Co., Ltd., Japan) with the surface area of 3 mm^2. Ag/AgCl reference electrode was prepared by coating Ag/AgCl ink on Au electrode and dried for 30 min in ambient atmosphere. The working and reference electrodes were separated by a distance of 5 mm. The various sputtering parameters like argon (Ar) flow rate, sputtering time, distance between substrate to target, and microwave power for Au and ZnO thin films were given in Table 1.

2.2. Microfluidic Device Fabrication and Measurement Setup. The complete microfluidic device fabrication scheme is given in Figure 1. At first, SU-8 2100 photoresist was spin-coated on Si wafer and subjected to UV exposure through photomask with the desired microfluidic channel pattern to create a master mold. UV exposure dose was maintained at 260 mJ/cm^2. Furthermore, the pattern was developed in the etching solution. PDMS and cross-linker (Sylgard 184) were mixed in the ratio of 10:2 and poured onto the master mold, then degassed and cured at 70 °C for overnight. Finally, the cured PDMS was peeled off from the master mold and bonded with glass substrates predeposited with working and reference electrodes using plasma bonding. The microfluidic channel is 140 μm wide, 70 μm wide, and 30 mm long. Entry and exit holes were made in the size of 2 mm using small puncher. Then, silicone tubes were attached on both holes, and pH buffer solutions were carefully passed through the microfluidic channel using a syringe pump. Next, pH-sensing studies were conducted using a two-electrode configuration setup. The potential differences between working and reference electrodes with respect to various pH buffer solutions (Horiba, Japan) were measured by using pH/mV meter (CL-9D02, Chemical Equipment Co., Ltd., Japan).

2.3. Characterization Techniques. The structural studies were characterized using X-ray diffraction (XRD) (LabX XRD 6100, Shimadzu, Japan) and X-ray photoelectron spectroscopy (XPS) (PHI Quantum 2000, Physical Electronics, Inc., USA). Morphological and topographical studies were analyzed using field-emission scanning electron microscopy (FE-SEM) (JEOL, JCM 6000, Japan) and laser microscopy (VK-X200, Keyence, USA). The elemental composition of ZnO thin film was analyzed using energy dispersive X-ray analysis (EDS). Morphological images of the cells (A7r5, A549, and MDCK) were taken under an inverted microscope (Eclipse Ti, NIKON Instruments Inc., USA).

3. RESULTS AND DISCUSSION

3.1. Structural Studies. Crystal structure of the ZnO thin film was analyzed using XRD and the diffraction pattern is shown in Figure 2a. The diffraction peaks were indexed according to Powder Diffraction File (PDF) no. 36−1451 (International Center for Diffraction Data (ICDD), 2006), which corresponds to hexagonal wurtzite structure. The prominent diffraction peaks at 34.14, 36.17, and 47.48° corresponds to (002), (101), and (102) planes, respectively. The high intensity (002) crystal plane indicates that the crystal grows along the *C*-axis which is perpendicular to the surface of the substrate. The other diffraction peaks ((101) and (102)) revealed that some crystallites were grown at random orientation. The crystallite size is evaluated using Scherrer's formula[44,45] (eq 1) as

DOI: 10.1021/acsami.6b16261
ACS Appl. Mater. Interfaces 2017, 9, 5193−5203

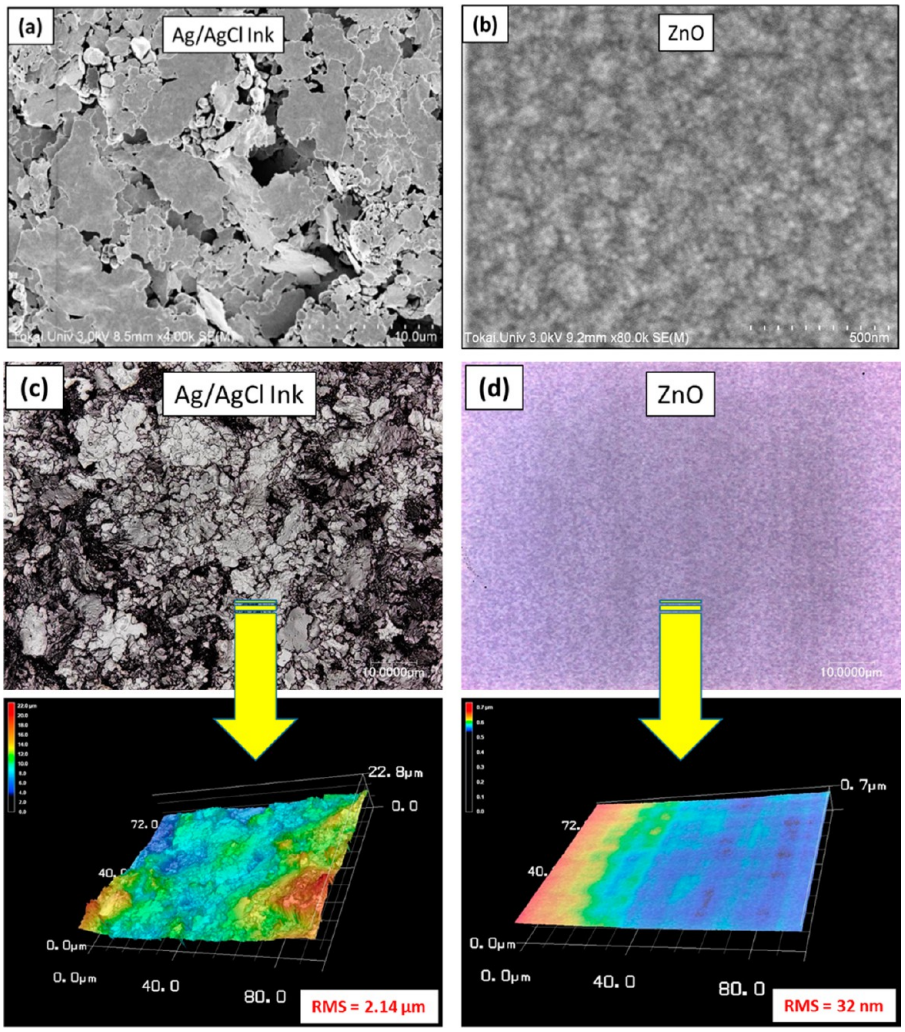

Figure 3. FESEM images of the (a) Ag/AgCl ink and (b) ZnO thin film. Topography and surface roughness of the (c) ZnO thin film and (d) Ag/AgCl ink.

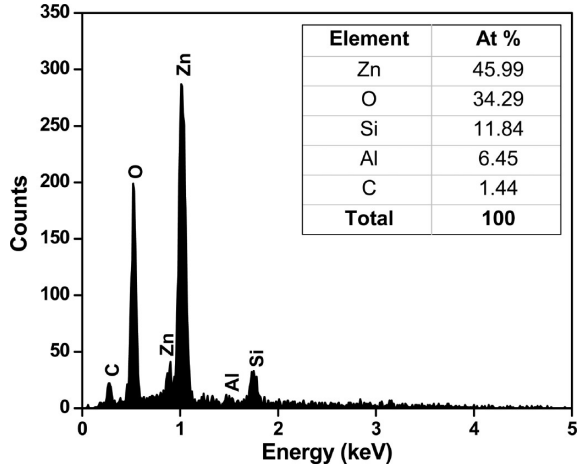

Figure 4. EDS spectra of the ZnO thin film.

$$D = \frac{0.94\lambda}{\beta \cos \theta} \quad (1)$$

where 0.94 is the shape factor for spheres, λ is the wavelength of the X-ray, β is the full width half-maximum of dominant crystal plane (002) in radians, and θ is the diffraction angle ((002) crystal plane). The estimated crystallite was size was found to be 8 nm. XPS measurements for ZnO thin film have been carried out after etching a surface about 20 nm with an Ar ion beam in order to eliminate the atmospheric contaminants. XPS survey scan spectra is shown in Figure 2b. The spectrum solely shows the elements such as Zn and O without any impurities, confirming the high purity of the deposited film. Zn core level peaks (Figure 2c) found at 1020.88 and 1043.94 eV are attributed to $2p_{3/2}$ and $2p_{1/2}$, respectively. The binding energy difference between $2p_{3/2}$ and $2p_{1/2}$ is 23.06 eV which confirms the phase confirmation of ZnO.[46] O 1s core level spectra is shown in Figure 2d. Two Gaussians peaks fitted for O 1s spectra positioned at 529.26 and 531.12 eV. The lower binding energy at 529.26 eV is assigned to O^{2-} ions in the Zn−O bonding of the wurtzite ZnO crystal structure.[47] The binding energy surrounding 531.12 eV corresponds to O^{2-} ions in the oxygen deficient regions within the matrix of ZnO.[48]

3.2. Morphological, Elemental and Topographical Analysis. The morphology of ZnO thin film and Ag/AgCl was analyzed using FE-SEM and laser microscope as shown in Figure 3a−d. Ag/AgCl micrographs (Figure 3a) depicted that unevenly sized sheetlike morphology accumulated randomly. The ZnO micrographs (Figure 3b) clearly revealed that high-quality, crack-free homogeneous microstructure. The mean

DOI: 10.1021/acsami.6b16261
ACS Appl. Mater. Interfaces 2017, 9, 5193−5203

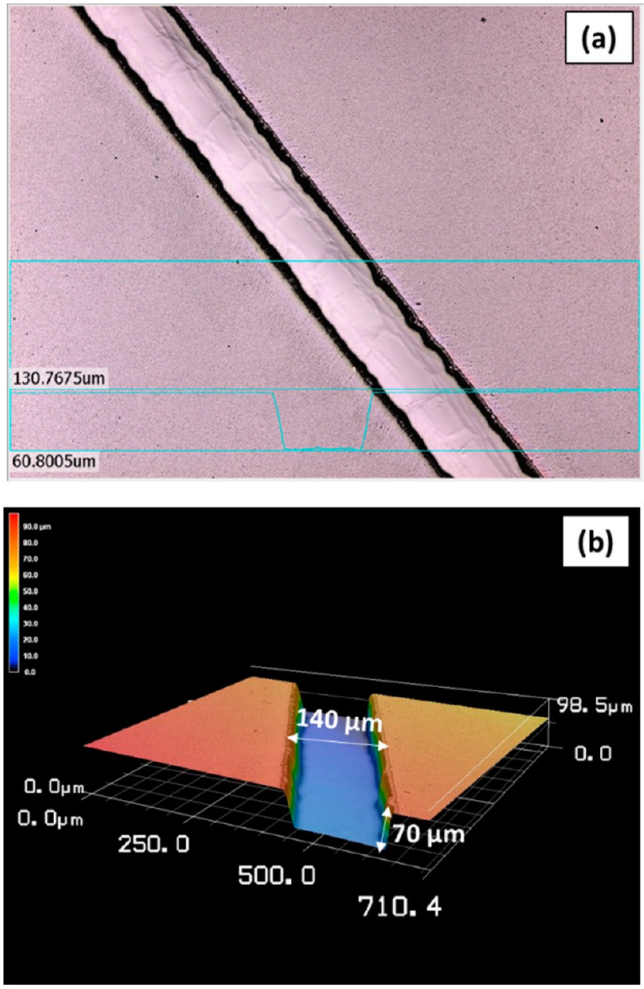

Figure 5. (a) Optical and (b) 3D image of the microfluidic channel.

diameter of 50 nm grains were evenly distributed throughout the films. To understand more about Ag/AgCl and ZnO, the surface topography (Figure 3c,d) has been monitored by laser microscope to determine the film roughness. The average roughness (RMS) of the scanned surface area of 50 μm by 50 μm for ZnO thin film was around 32 nm, and for Ag/AgCl, it was around 2.14 μm. Figure 4 shows the EDS spectra of the ZnO thin film. The sample contains Zn, O, Si, Al, and C. The presence of little C is from atmospheric contents or may be from the carbon tape. The Al and Si may arose from the substrate. Elemental mapping of the Zn and O revealed the nonstoichiometric oxygen deficiency. Figure 5a,b shows the topography of the microfluidic channel. The microfluidic channel is 140 μm in wide, 70 μm in depth, and 30 mm long.

3.3. pH Sensing Studies. In the following, we demonstrated the pH-sensing studies of the microfluidic device fabricated using Ag/AgCl and ZnO thin films. The testing procedure schematic of the microfluidic pH sensor is presented in Figure 6a. The photograph of the final developed device is shown in Figure 6b. pH-sensing studies were done by potentiometric method according the potential difference between the reference electrode (Ag/AgCl) and working electrode (ZnO). First, after plasma bonding of the PDMS mold with electrodes, the microfluidic device was sterilized with ethanol and washed with deionized water after each pH test. The pH level of each test solution was confirmed by a commercial pH glass electrode. The sensitivity of the developed microfluidic device was validated by passing various pH buffer solutions for a period of time at room temperature through the microfluidic channel with the support of syringe pump. We tested the pH-sensing capability of the developed microfluidic device with the flow rate of 120 μL/min thrice in various pH solutions in order to validate the sensitivity, reproducibility, and stability behaviors. The tests began with the most acidic buffer (pH 1.68) and increased gradually to the most alkaline buffer (pH 9.18).

3.3.1. Sensitivity. Figure 7a shows the potential responses of four different pH solutions from 1.68 to 9.18. To confirm consistency, the tests were done three times. The three test results showed the sensitivities of −43.25, −43.22, and −44.23 mV/pH with correlation coefficients of 0.9599, 0.9590, and 0.9679, respectively. Figure 7b shows the pH responses tested in reversible order with four different solutions from 9.18 to 1.68. The three test results showed the sensitivities of −43.63, −43.35, and −44.59 mV/pH with correlation coefficients of 0.9648, 0.9555, and 0.9417, respectively. Nearly identical values were obtained in all three tests. The pH versus voltage curve exhibited high linearity over a wide pH range with an average sensitivity of −43.7116 mV/pH. The potential difference in each pH solution stayed almost constant with minimal drift of ±3 mV/hour. Moreover, the minimal drifts were very small when compared with the potential changes to recognize various pH levels. According to previous literatures, potential deviation less than ±5 mV is acceptable in many cases.[22,49,50]

3.3.2. Flow Rate and Stability. The developed microfluidic device exhibited high sensitivity throughout a wide pH range. Apart from sensitivity, there are several key parameters that need to be considered when selecting the sensor for real time application. In the case of microfluidic devices, sensor stability and the effect of flow rate are extremely important to maintain the usage of sensor over long time. The output characteristics with respect to flow rate from 24 to 120 μL/min is shown in Figure 7c. The results indicated that no significant change was observed with various flow rates. To check the stability of the device, time domain pH monitoring for continuous usage was recorded over a short time period, and the results were shown in Figure 7d. The flow rate and stability studies demonstrate that good reliability and durability of the microfluidic device over a wide range of flow speed over a long period of time. Long-term stability of the sensor allow manufacturers to build sensor with minimum calibration which also reduces the total cost of the sensor.

3.3.3. Response Time. Response time of the microfluidic pH sensor of each pH buffer solutions were tested. Generally, response time is defined as time taken to attain 90% of its stable potential.[50] Before measurement the microfluidic channel was flushed with water and air.

Figure 8a−d shows typical response time characteristics of the microfluidic sensor. This implies that the time taken to reach stable potential was short. A rapid step change was noticed once the pH solution passed through the microfluidic device. After 3 similar experiments, we concluded that the average response time was 29 s. The quicker response time resulted in minimizing the total analysis time.

3.4. pH-Sensing Mechanism. Usually metal oxides will get hydrolyzed in the presence of water to form hydroxide on the surface. The polar hydroxyl (−OH) groups may cause the surface to attract and physically adsorb a single layer or several

DOI: 10.1021/acsami.6b16261
ACS Appl. Mater. Interfaces 2017, 9, 5193−5203

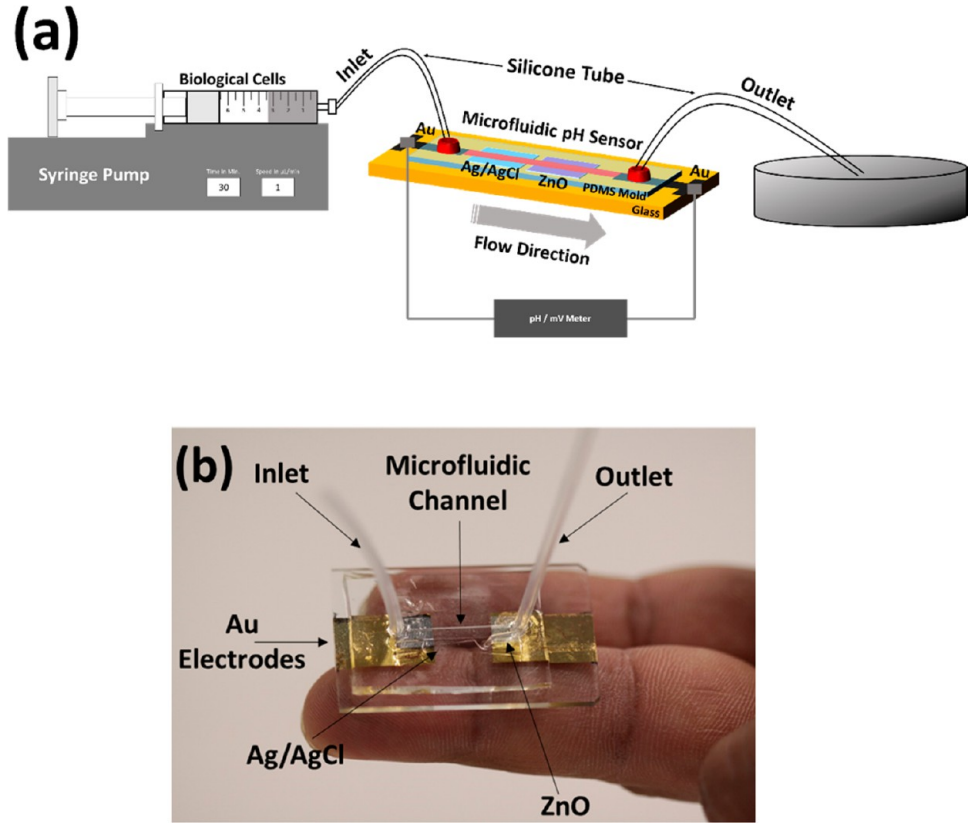

Figure 6. (a) Experimental scheme of the pH measurement setup and (b) photograph of the fabricated microfluidic device.

additional layers of polar water molecules. When ZnO surface interacts with an electrolyte, surface charge will develop through various mechanisms like adsorption of ions, accumulation/depletion of charge species at the surface, or physical adsorption of charged species on the surface. At first, H^+-specific binding sites present on ZnO can hydrogenate after contact with electrolyte solution. These binding sites can protonate or deprotonate resulting in a change in surface charge according to electrolyte pH.[25,26] Since ZnO is an amphoteric oxide, it is not surprising that it can react with both acidic and basic solutions. The probable acid and base reactions (eqs 2 and 3) on ZnO surface are given as[26]

For acid:

$$ZnO + 2OH^- + H_2O \rightarrow Zn(OH)_4^{2-} \quad (2)$$

For base:

$$ZnO + 2H_3O^+ + 3H_2O \rightarrow Zn(H_2O)_6^{2+} \quad (3)$$

The potentiometric device constructed here using Ag|AgCl| Cl^- as a reference electrode supplied at constant potential against ZnO thin film electrode. The overall structure of the potential cell (eq 4) in this research work was as follows:

$$Au|ZnO|Test\ Electrolyte\ Cl^-|AgCl|Au \quad (4)$$

According to the Nernst equation,[34] the standard electrode potential can be denoted as

$$E = E_0 - \frac{2.303RT}{F}pH \quad (5)$$

where E_0 is the standard ZnO electrode potential, R is the universal gas constant (8.314 J/mol K), T is the absolute temperature (298 K), and F is the Faraday constant (96 487.3415 C mol^{-1}). At room temperature, the Nernst equation gave a slope value of 59.1 mV/pH. As shown in Figure 7a,b, the potential difference of the ZnO thin film is linearly dependent on the pH value of buffer solutions ranging from 1.68 to 9.18. Even though the obtained sensitivity was lower than the theory value, minimum electrolyte solution, quick response time, and minimal drift with respect to flow rate mark this developed device distinctive. The sensitivity of the ZnO thin film largely depends on its surface to volume ratio and oxygen vacancies. EDS mapping also evidence of more oxygen vacancy (Zn/O = 45.99:34.29 atom %) in ZnO thin film which resulted in increasing number of binding sites for electrochemical processes. The unsaturated dangling bonds at the surface are usually compensated by reactive molecules such as H_2O and favors for more adsorption/desorption process.[51] Since ZnO has a high density of binding sites for H^+ and OH^-, at lower pH levels (<7), the potential difference is high due to greater diffusion of (H^+) on ZnO surface, but at higher pH levels (>7), the potential difference is low due to ZnO losing a proton from OH^- and forming a negatively charged surface.[32] Also, it is worth noting that this kind of electrode could work well in the highly corrosive systems due to its wide sensing range. Compared to the response times of a few minutes in other reports, the response of our sensor was shorter and reliable compared with different pH solutions. This may be due to not only solid−liquid interaction in the much closed channel but also the absence of environmental turbulences. The high sensitivity of the ZnO thin film may be attributed due to smaller grains which can provide more active area and polycrystalline nature of the films resulted in high oxygen vacancies could assist to sense

DOI: 10.1021/acsami.6b16261
ACS Appl. Mater. Interfaces 2017, 9, 5193−5203

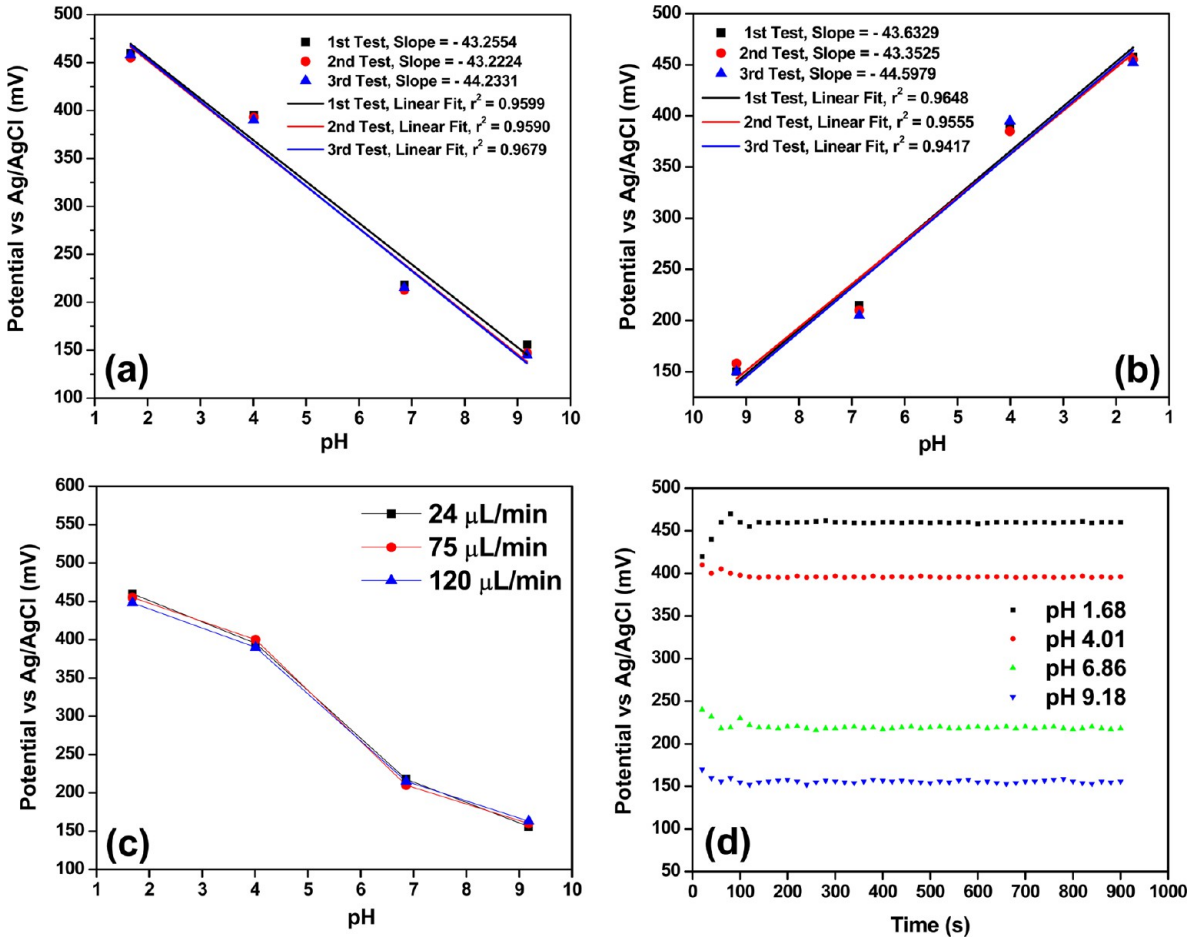

Figure 7. pH-sensing responses (a) from 1.68 to 9.18, (b) from 9.18 to 1.68. (c) Flow rate studies with respect to various pH solutions and (d) stability nature of the developed microfluidic device.

H^+ concentration.[52] The overall sensing performance of the developed devices is compared with the available literature reports based on ZnO, and the same is shown in Table 2. This clearly tells us that the microfluidic device has the high sensitivity, high stability, and short response time with a small amount of liquid.

4. *IN VITRO* EVALUATION

One of the most important criteria in order to verify the quality of the developed CTC recognition device is *in vitro* testing. Therefore, to evaluate the capability to differentiate the difference between three cells (A549, A7r5, and MDCK), a model was proposed and evaluated. A549 human lung cancer cells (CCL-185, ATCC), A7r5 rat embryonic aortic smooth muscle cells (CRL1444, ATCC), and MDCK dog kidney cells (CCL-34, ATCC) were cultured in low-glucose (1 g/L) DMEM (Gibco) supplemented with 10% fetal bovine serum (SAFC Biosciences), 1% antibiotic−antimycotic, and 1% nonessential amino acids (Gibco). Cells were maintained in a 5% CO_2 incubator at 37 °C. Cells were adjusted to a density of 1×10^5 cells/mL in the medium. The low- and high-magnification microscope images of the cells were shown in Figure 9a−f. Prior to conducting experiments, the on-chip inlet and outlet probes were connected with cell culture vials and syringe pump. The cells were introduced in to the microfluidic chip via high-purity tubing driven by syringe pump. To provide optimum temperature and sterile environment of the cells, the microfluidic device and cultured cells vials were kept inside the CO_2 incubator. The flow rate of the cells were set at 120 μL/min. As apparent from the real-time cells data (Figure 9g), the developed device has the ability to differentiate the three different cells having different pH values. Since the size of the A7r5 cells is very large (<100 μm), the number of cells that can pass through the channel is limited resulted in poor response. Likewise, we can see the clear difference between the DMEM medium and DMEM medium containing cells (A549 and MDCK). Also, the A549 and MDCK cells are smaller (<10 μm) than A7r5 cells, leading to large potential difference in the sensor. There are still much more detailed experiments and modeling is in progress to clearly understand the interaction of various cells with ZnO surface.

5. CONCLUSION

In this paper, we successfully fabricated a microfluidics-based pH sensor using rf sputtered ZnO thin films and Ag/AgCl ink. The fabricated sensor exhibited the super-Nernstian response of 48 mV/pH. Undoubtedly, quick detection time and enhanced measurement capability provided by the developed microfluidic device is a valuable additional tool to identify CTCs in the blood either with or without DLD devices. The pH-sensing measurements show reproducible potentials for each pH value with shorter response times. The fabricated pH sensor exhibits

DOI: 10.1021/acsami.6b16261
ACS Appl. Mater. Interfaces 2017, 9, 5193−5203

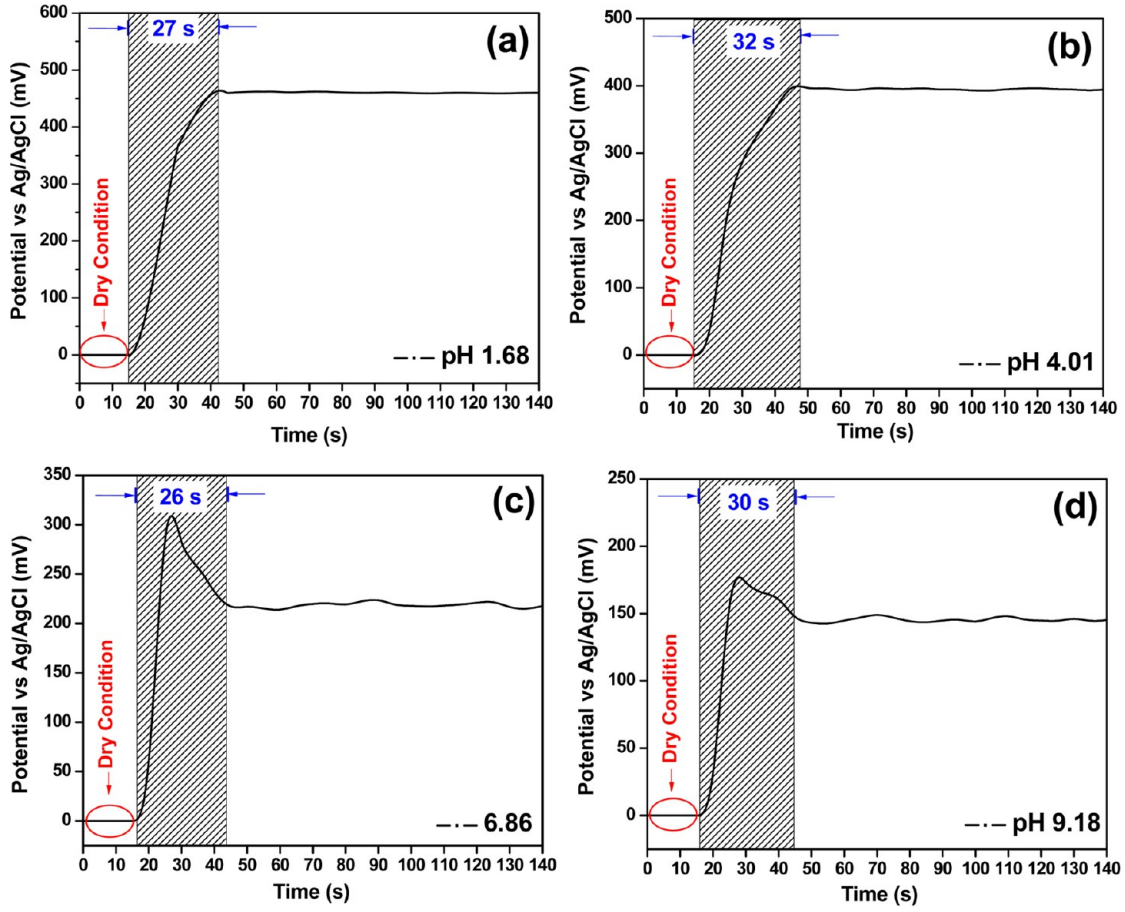

Figure 8. Response time analysis with respect to various pH buffer solutions (a) 1.68, (b) 4.01, (c) 6.86, and (d) 9.18.

Table 2. Comparison of ZnO-Based pH Sensor Performance with the Present Research Work

sensor types	sensor materials	pH range	sensitivity (mV/pH)	response time (s)	electrolyte volume	references
extended gate field effect transistor	ZnO thin film	2−12	38		immersed in electrolyte	53
extended gate field effect transistor	coaxial-structured ZnO/silicon nanowire	1−13	46.25		immersed in electrolyte	54
shear horizontal surface acoustic wave	ZnO nanoparticle	2−7			immersed in electrolyte	30
extended gate field effect transistor	In−Ga−ZnO nanoparticle/Si nanowire	2−10	50	60	immersed in electrolyte	55
interdigitated electrode array	ZnO thin film	2−10	3.72	5	2 mL	56
intracellular	ZnO nanotube	4−12	−45.9	300	immersed in electrolyte	57
biological species	ZnO nanorod	4−12	−28.4	300	immersed in electrolyte	57
extended gate field effect transistor	passivated intrinsic zinc oxide nanorod	4−12	44.01		immersed in electrolyte	58
extended gate sensing	zinc oxide nanorod	4−12	53.55		immersed in electrolyte	59
electrochemical	iridium oxide	1.5−12	−51.7	2	immersed in electrolyte	22
extended gate field effect transistor	amorphous indium−gallium zinc oxide	3−10	59.2	less than 300	immersed in electrolyte	60
extended gate field effect transistor	ZnO−Ta thin film	1.3−12	41.56		immersed in electrolyte	61
potentiometric	**ZnO thin film**	**2−9**	**43.71**	**29**	**5 mL**	**present work**

several advantages like simple processing steps which appropriate for mass production. Furthermore, in near future, we will try to attempt to identify CTCs in blood using the fabricated device. The ability to provide a high sensitivity, negligible effect

DOI: 10.1021/acsami.6b16261
ACS Appl. Mater. Interfaces 2017, 9, 5193−5203

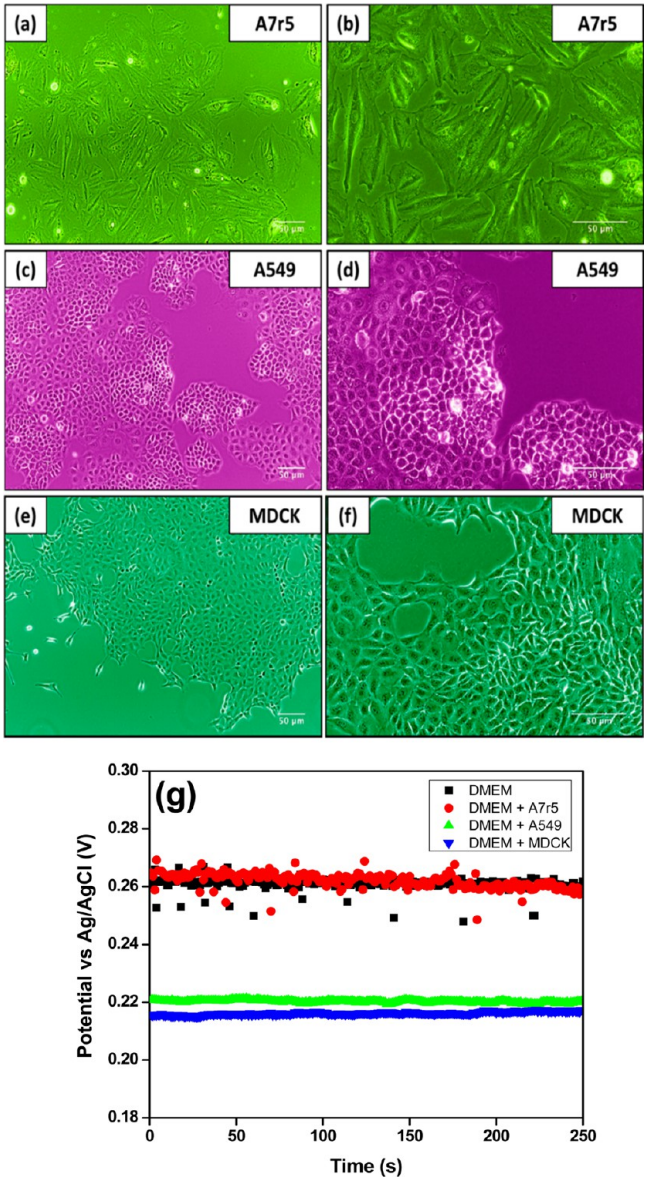

Figure 9. Inverted microscope low- and high-magnification images of (a and b) A7r5, (c and d) A549, (e and f) MDCK cells, and (g) pH-sensing responses of the microfluidic device with various cells.

on microfluidic flow rate, and high stability are the key impact of this research work.

AUTHOR INFORMATION

Corresponding Author

*Tel.: +81 463 58 1211 ext. 4791. Fax: +81 0463 50 2480. E-mail: ganesh@tsc.u-tokai.ac.jp; ganeshkumarmani@hotmail.com.

ORCID

Ganesh Kumar Mani: 0000-0003-0046-4676

Notes

The authors declare no competing financial interest.

ACKNOWLEDGMENTS

Authors wish to express their sincere thanks to the Micro/Nano Technology Center (MNTC), Tokai University (Shonan Campus), Japan for their infrastructural and financial support. Also authors express their sincere thanks to Tokai Imaging Center for Advanced Research (TICAR), Tokai University (Shonan campus), Japan for additional characterization techniques.

REFERENCES

(1) Adams, D. L.; Stefansson, S.; Haudenschild, C.; Martin, S. S.; Charpentier, M.; Chumsri, S.; Cristofanilli, M.; Tang, C. M.; Alpaugh, R. K. Cytometric Characterization of Circulating Tumor Cells Captured by Microfiltration and Their Correlation to the Cellsearch?? CTC Test. *Cytometry, Part A* **2015**, *87* (2), 137−144.

(2) Warkiani, M. E.; Khoo, B. L.; Wu, L.; Tay, A. K. P.; Bhagat, A. A. S.; Han, J.; Lim, C. T. Ultra-Fast, Label-Free Isolation of Circulating Tumor Cells from Blood Using Spiral Microfluidics. *Nat. Protoc.* **2015**, *11* (1), 134−148.

(3) Madhurantakam, S.; Jayanth Babu, K.; Balaguru Rayappan, J. B.; Krishnan, U. M. Fabrication of Mediator-Free Hybrid Nano-Interfaced Electrochemical Biosensor for Monitoring Cancer Cell Proliferation. *Biosens. Bioelectron.* **2017**, *87*, 832−841.

(4) Dolfus, C.; Piton, N.; Toure, E.; Sabourin, J.-C. Circulating Tumor Cell Isolation: The Assets of Filtration Methods with Polycarbonate Track-Etched Filters. *Chin. J. Cancer Res.* **2015**, *27* (5), 479−487.

(5) Hyun, K.-A.; Lee, T. Y.; Lee, S. H.; Jung, H.-I. Two-Stage Microfluidic Chip for Selective Isolation of Circulating Tumor Cells (CTCs). *Biosens. Bioelectron.* **2015**, *67*, 86−92.

(6) Huang, T.; Jia, C.-P.; Jun-Yang; Sun, W.-J.; Wang, W.-T.; Zhang, H.-L.; Cong, H.; Jing, F.-X.; Mao, H.-J.; Jin, Q.-H.; Zhang, Z.; Chen, Y.-J.; Li, G.; Mao, G.-X.; Zhao, J.-L. Highly Sensitive Enumeration of Circulating Tumor Cells in Lung Cancer Patients Using a Size-Based Filtration Microfluidic Chip. *Biosens. Bioelectron.* **2014**, *51*, 213−218.

(7) Loutherback, K.; D'Silva, J.; Liu, L.; Wu, A.; Austin, R. H.; Sturm, J. C. Deterministic Separation of Cancer Cells from Blood at 10 mL/min. *AIP Adv.* **2012**, *2* (4), 042107.

(8) Stott, S. L.; Hsu, C.-H. C.-H.; Tsukrov, D. I.; Yu, M.; Miyamoto, D. T.; Waltman, B. a.; Rothenberg, S. M.; Shah, A. M.; Smas, M. E.; Korir, G. K.; Floyd, F. P.; Gilman, A. J.; Lord, J. B.; Winokur, D.; Springer, S.; Irimia, D.; Nagrath, S.; Sequist, L. V.; Lee, R. J.; Isselbacher, K. J.; Maheswaran, S.; Haber, D. a.; Toner, M. Isolation of Circulating Tumor Cells Using a Microconvortex-Generating Herringbone-Chip. *Proc. Natl. Acad. Sci. U. S. A.* **2010**, *107* (35), 18392−18397.

(9) Sarioglu, a F.; Aceto, N.; Kojic, N.; Donaldson, M. C.; Zeinali, M.; Hamza, B.; Engstrom, A.; Zhu, H.; Sundaresan, T. K.; Miyamoto, D. T.; Luo, X.; Bardia, A.; Wittner, B. S.; Ramaswamy, S.; Shioda, T.; Ting, D. T.; Stott, S. L.; Kapur, R.; Maheswaran, S.; Haber, D. a; Toner, M. A Microfluidic Device for Label-Free, Physical Capture of Circulating Tumor Cell Clusters. *Nat. Methods* **2015**, *12* (April), 685−691.

(10) Griffiths, J. R. Are Cancer Cells Acidic? *Br. J. Cancer* **1991**, *64* (April), 425−427.

(11) Damaghi, M.; Wojtkowiak, J. W.; Gillies, R. J. pH Sensing and Regulation in Cancer. *Front. Physiol.* **2013**, *4*, 370.

(12) Del Ben, F.; Turetta, M.; Celetti, G.; Piruska, A.; Bulfoni, M.; Cesselli, D.; Huck, W. T. S.; Scoles, G. A Method for Detecting Circulating Tumor Cells Based on the Measurement of Single-Cell Metabolism in Droplet-Based Microfluidics. *Angew. Chem., Int. Ed.* **2016**, *55*, 8581−8584.

(13) Swietach, P.; Vaughan-Jones, R. D.; Harris, A. L.; Hulikova, A. The Chemistry, Physiology and Pathology of pH in Cancer. *Philos. Trans. R. Soc., B* **2014**, *369* (1638), 20130099.

(14) Kaneko, D.; Tsuchiya, K. Development of the Micro Region pH Sensor Using Ag/$AgIO_3$ Electrode Method. *International Symposium on Micro-NanoMechatronics and Human Science (MHS)* **2013**, 1−4.

(15) Kaneko, D.; Tsuchiya, K. Development of the Micro Region pH Sensor Using Ag/$AgIO_3$ Electrode Method. *Int. Symp. Micro-NanoMechatronics Hum. Sci.* **2013**, 1−4.

DOI: 10.1021/acsami.6b16261
ACS Appl. Mater. Interfaces 2017, 9, 5193−5203

(16) Chaniotakis, N.; Fouskaki, M. Bio-Chem-FETs: Field Effect Transistors for Biological Sensing. *Biological Identification* **2014**, 194–219.
(17) Bubendorfer, A. J.; Ingham, B.; Kennedy, J. V.; Arnold, W. M. Contamination of PDMS Microchannels by Lithographic Molds. *Lab Chip* **2013**, *13* (22), 4312–4316.
(18) Menzel, A.; Subannajui, K.; Güder, F.; Moser, D.; Paul, O.; Zacharias, M. Multifunctional ZnO-Nanowire-Based Sensor. *Adv. Funct. Mater.* **2011**, *21* (22), 4342–4348.
(19) Kang, B. S.; Ren, F.; Heo, Y. W.; Tien, L. C.; Norton, D. P.; Pearton, S. J. pH Measurements with Single ZnO Nanorods Integrated with a Microchannel. *Appl. Phys. Lett.* **2005**, *86* (11), 112105.
(20) Kaviyarasu, K.; Geetha, N.; Kanimozhi, K.; Maria Magdalane, C.; Sivaranjani, S.; Ayeshamariam, A.; Kennedy, J.; Maaza, M. In Vitro Cytotoxicity Effect and Antibacterial Performance of Human Lung Epithelial Cells A549 Activity of Zinc Oxide Doped TiO_2 Nanocrystals: Investigation of Bio-Medical Application by Chemical Method. *Mater. Sci. Eng., C* **2016**, DOI: 10.1016/j.msec.2016.12.024.
(21) Santos, L.; Neto, J. P.; Crespo, A.; Nunes, D.; Costa, N.; Fonseca, I. M.; Barquinha, P.; Pereira, L.; Silva, J.; Martins, R.; Fortunato, E. WO_3 Nanoparticle-Based Conformable pH Sensor. *ACS Appl. Mater. Interfaces* **2014**, *6*, 12226–12234.
(22) Huang, W. D.; Cao, H.; Deb, S.; Chiao, M.; Chiao, J. C. A Flexible pH Sensor Based on the Iridium Oxide Sensing Film. *Sens. Actuators, A* **2011**, *169* (1), 1–11.
(23) Qingwen, L.; Yiming, W.; Guoan, L. pH-Response of Nanosized MnO2 Prepared with Solid State Reaction Route at Room Temperature. *Sens. Actuators, B* **1999**, *59* (1), 42–47.
(24) Sardarinejad, A.; Maurya, D.; Alameh, K. The pH Sensing Properties of RF Sputtered RuO2 Thin-Film Prepared Using Different Ar/O_2 Flow Ratio. *Materials* **2015**, *8* (6), 3352–3363.
(25) Al-Hilli, S. M.; Al-Mofarji, R. T.; Klason, P.; Willander, M.; Gutman, N.; Sa'Ar, A. Zinc Oxide Nanorods Grown on Two-Dimensional Macroporous Periodic Structures and Plane Si as a pH Sensor. *J. Appl. Phys.* **2008**, *103* (1), 014302.
(26) Al-Hilli, S. M.; Al-Mofarji, R. T.; Willander, M. Zinc Oxide Nanorod for Intracellular pH Sensing. *Appl. Phys. Lett.* **2006**, *89* (17), 173119.
(27) Nesakumar, N.; Sethuraman, S.; Krishnan, U. M.; Rayappan, J. B. B. Electrochemical Acetylcholinesterase Biosensor Based on ZnO Nanocuboids Modified Platinum Electrode for the Detection of Carbosulfan in Rice. *Biosens. Bioelectron.* **2016**, *77*, 1070–1077.
(28) Saasa, V.; Mokwena, M.; Dhonge, B.; Manikandan, E.; Kennedy, J.; Murmu, P. P.; Dewar, J.; Erasmus, R.; Whaley, M. F.; Mukwevho, E. Bonex Mwakikunga. Optical and Structural Properties of Multi-Wall-Carbon-Nanotube-Modified ZnO Synthesized at Varying Substrate Temperatures for Highly Efficient Light Sensing Devices. *Sens. Transducers J.* **2015**, *195* (12), 9–17.
(29) Lokesh, K.; Kavitha, G.; Manikandan, E.; Mani, G. K.; Kaviyarasu, K.; Rayappan, J. B. B.; Ladchumananandasivam, R.; Sundeep Aanand, J.; Jayachandran, M.; Maaza, M. Effective Ammonia Detection Using N-ZnO/p-NiO Heterostructured Nanofibers. *IEEE Sens. J.* **2016**, *16* (8), 2477–2483.
(30) Oh, H.; Lee, K. J.; Baek, J.; Yang, S. S.; Lee, K. Development of a High Sensitive pH Sensor Based on Shear Horizontal Surface Acoustic Wave with ZnO Nanoparticles. *Microelectron. Eng.* **2013**, *111*, 154–159.
(31) Copa, V.; Tuico, A.; Mendoza, J.; Ferrolino, J.; Vergara, C.; Salvador, A.; Estacio, E.; Somintac, A. Development of Resistance-Based pH Sensor Using Zinc Oxide Nanorods. *J. Nanosci. Nanotechnol.* **2016**, *16* (6), 6102–6106.
(32) Haarindraprasad, R.; Hashim, U.; Gopinath, S. C. B.; Kashif, M.; Veeradasan, P.; Balakrishnan, S. R.; Foo, K. L.; Poopalan, P. Low Temperature Annealed Zinc Oxide Nanostructured Thin Film-Based Transducers: Characterization for Sensing Applications. *PLoS One* **2015**, *10* (7), e0132755.
(33) Mukhiya, R.; Sharma, R.; Khanna, V. K.; Adami, A.; Lorenzelli, L.; Zen, M. RF-Sputtered, Nanostructured ZnO-Based Extended-Gate Field-Effect Transistor as pH Sensor. *Sens. Lett.* **2015**, *13* (1), 26–31.
(34) Maiolo, L.; Mirabella, S.; Maita, F.; Alberti, A.; Minotti, A.; Strano, V.; Pecora, A.; Shacham-Diamand, Y.; Fortunato, G. Flexible pH Sensors Based on Polysilicon Thin Film Transistors and ZnO Nanowalls. *Appl. Phys. Lett.* **2014**, *105* (9), 093501.
(35) Mani, G. K.; Rayappan, J. B. B. Selective Recognition of Hydrogen Sulfide Using Template and Catalyst Free Grown ZnO Nanorods. *RSC Adv.* **2015**, *5* (68), 54952–54962.
(36) Mani, G. K.; Rayappan, J. B. B. A Highly Selective Room Temperature Ammonia Sensor Using Spray Deposited Zinc Oxide Thin Film. *Sens. Actuators, B* **2013**, *183*, 459–466.
(37) Dhivya, P.; Prasad, A. K.; Sridharan, M. Nanostructured TiO_2 Films: Enhanced NH3 Detection at Room Temperature. *Ceram. Int.* **2014**, *40* (1), 409–415.
(38) Manikandan, E.; Murugan, V.; Kavitha, G.; Babu, P.; Maaza, M. Nanoflower Rod Wire-like Structures of Dual Metal (Al and Cr) Doped ZnO Thin Films: Structural, Optical and Electronic Properties. *Mater. Lett.* **2014**, *131*, 225–228.
(39) Mendelsberg, R. J.; Kennedy, J.; Durbin, S. M.; Reeves, R. J. Carbon Enhanced Blue–violet Luminescence in ZnO Films Grown by Pulsed Laser Deposition. *Curr. Appl. Phys.* **2008**, *8* (3), 283–286.
(40) Liu, Z.; Fan, T.; Zhang, D.; Gong, X.; Xu, J. Hierarchically Porous ZnO with High Sensitivity and Selectivity to H_2S Derived from Biotemplates. *Sens. Actuators, B* **2009**, *136* (2), 499–509.
(41) Kennedy, J.; Murmu, P. P.; Leveneur, J.; Markwitz, A.; Futter, J. Controlling Preferred Orientation and Electrical Conductivity of Zinc Oxide Thin Films by Post Growth Annealing Treatment. *Appl. Surf. Sci.* **2016**, *367*, 52–58.
(42) Zhang, X. Q.; Suemune, I.; Kumano, H.; Yao, Z. G.; Huang, S. H. Room Temperature Ultraviolet Lasing Action in High-Quality ZnO Thin Films. *J. Lumin.* **2007**, *122–123* (1–2), 828–830.
(43) Shankar, P.; Rayappan, J. B. B. Racetrack Effect on the Dissimilar Sensing Response of ZnO Thin Film—An Anisotropy of Isotropy. *ACS Appl. Mater. Interfaces* **2016**, *8*, 24924.
(44) Pandiadurai, K.; Mani, G. K.; Shankar, P.; Rayappan, J. B. B. ZnO Nanospheres to Nanorods – Morphology Transition via Fe-Doping. *Superlattices Microstruct.* **2013**, *62*, 39–46.
(45) Thanigai Arul, K.; Manikandan, E.; Ladchumananandasivam, R.; Maaza, M. Novel Polyvinyl Alcohol Polymer Based Nanostructure with Ferrites Co-Doped with Nickel and Cobalt Ions for Magneto-Sensor Application. *Polym. Int.* **2016**, *65* (12), 1482–1485.
(46) Joshi, A. G.; Sahai, S.; Gandhi, N.; Krishna, Y. G. R.; Haranath, D. Valence Band and Core-Level Analysis of Highly Luminescent ZnO Nanocrystals for Designing Ultrafast Optical Sensors. *Appl. Phys. Lett.* **2010**, *96*, 123102.
(47) Sundara Venkatesh, P.; Balakumar, S.; Jeganathan, K. Post-Annealing Effects on the Structural and Optical Properties of Vertically Aligned Undoped ZnO Nanorods Grown by Radio Frequency Magnetron Sputtering. *RSC Adv.* **2014**, *4*, 5030–5035.
(48) Chen, M.; Wang, X.; Yu, Y. H.; Pei, Z. L.; Bai, X. D.; Sun, C.; Huang, R. F.; Wen, L. S. X-Ray Photoelectron Spectroscopy and Auger Electron Spectroscopy Studies of Al-Doped ZnO Films. *Appl. Surf. Sci.* **2000**, *158* (1), 134–140.
(49) Kreider, K. G.; Tarlov, M. J.; Cline, J. P. Sputtered Thin-Film pH Electrodes of Platinum, Palladium, Ruthenium, and Iridium Oxides. *Sens. Actuators, B* **1995**, *28* (3), 167–172.
(50) Yao, S.; Wang, M.; Madou, M. A pH Electrode Based on Melt-Oxidized Iridium Oxide. *J. Electrochem. Soc.* **2001**, *148* (4), H29–H36.
(51) Ghosh, M.; Karmakar, D.; Basu, S.; Jha, S. N.; Bhattacharyya, D.; Gadkari, S. C.; Gupta, S. K. Effect of Size and Aspect Ratio on Structural Parameters and Evidence of Shape Transition in Zinc Oxide Nanostructures. *J. Phys. Chem. Solids* **2014**, *75* (4), 543–549.
(52) Li, H. H.; Yang, C. E.; Kei, C. C.; Su, C. Y.; Dai, W. S.; Tseng, J. K.; Yang, P. Y.; Chou, J. C.; Cheng, H. C. Coaxial-Structured ZnO/silicon Nanowires Extended-Gate Field-Effect Transistor as pH Sensor. *Thin Solid Films* **2013**, *529*, 173–176.
(53) Batista, P. D.; Mulato, M. ZnO Extended-Gate Field-Effect Transistors as pH Sensors. *Appl. Phys. Lett.* **2005**, *87*, 143508.
(54) Li, H.; Yang, C.; Kei, C.; Su, C.; Dai, W.; Tseng, J.; Yang, P.-Y.; Chou, J.-C.; Cheng, H.-C. Coaxial-Structured ZnO/Silicon Nanowires

DOI: 10.1021/acsami.6b16261
ACS Appl. Mater. Interfaces 2017, 9, 5193–5203

Extended-Gate Field-Effect Transistor as pH Sensor. *Thin Solid Films* **2013**, *529*, 173−176.
(55) Lin, J.; Huang, B.; Yang, Y. IGZO Nanoparticle-Modified Silicon Nanowires as Extended-Gate Field-Effect Transistor pH Sensors. *Sens. Actuators, B* **2013**, *184*, 27−32.
(56) Haarindraprasad, R.; Hashim, U.; Gopinath, S. C. B.; Kashif, M.; Veeradasan, P.; Balakrishnan, S. R.; Foo, K. L.; Poopalan, P. Low Temperature Annealed Zinc Oxide Nanostructured Thin Film-Based Transducers: Characterization for Sensing Applications. *PLoS One* **2015**, *10*, e0132755.
(57) Fulati, A.; Usman Ali, S. M.; Riaz, M.; Amin, G.; Nur, O.; Willander, M. Miniaturized pH Sensors Based on Zinc Oxide Nanotubes/Nanorods. *Sensors* **2009**, *9*, 8911−8923.
(58) Chiu, Y.; Tseng, C.; Lee, C. Nanostructured EGFET pH Sensors With Surface-Passivated ZnO Thin-Film and Nanorod Array. *IEEE Sens. J.* **2012**, *12* (5), 930−934.
(59) Chiu, Y.; Lee, C. pH Sensor Investigation of Various-Length Photoelectrochemical Passivated ZnO Nanorod Arrays. *J. Electrochem. Soc.* **2011**, *158* (9), J282.
(60) Jang, H.; Gu, J.; Cho, W. Sensitivity Enhancement of Amorphous InGaZnO Thin Film Transistor Based Extended Gate Field-Effect Transistors with Dual-Gate Operation. *Sens. Actuators, B* **2013**, *181*, 880−884.
(61) Chiu, Y.; Lee, C.; Lou, L.; Ho, S.; Chuang, C. Wide Linear Sensing Sensors Using ZnO: Ta Extended-Gate Field-Effect-Transistors. *Sens. Actuators, B* **2013**, *188*, 944−948.

DOI: 10.1021/acsami.6b16261
ACS Appl. Mater. Interfaces 2017, 9, 5193−5203